Diffusion- and Perfusion-weighted MRI Radiomics for Survival Prediction in Patients with Lower-grade Gliomas

Chae Jung Park
Yonsei University Health System
Sooyon Kim
Yonsei University
Kyunghwa Han
Yonsei University Health System
Sung Soo Ahn
sungsoo@yuhs.ac
Yonsei University Health System
Dain Kim
Pohang University of Science and Technology
Yae Won Park
Yonsei University Health System
Jong Hee Chang
Yonsei University Health System
Se Hoon Kim
Yonsei University Health System
Seung-Koo Lee
Yonsei University Health System

Article

Keywords: Glioma, Isocitrate Dehydrogenase, Magnetic Resonance Imaging, Prognosis, Nomogram

Posted Date: June 22nd, 2022

DOI: https://doi.org/10.21203/rs.3.rs-1644727/v2

Additional Declarations: No competing interests reported.

Version of Record: A version of this preprint was published at Yonsei Medical Journal on January 1st, 2024. See the published version at https://doi.org/10.3349/ymj.2023.0323.

Abstract

Purpose

Lower-grade gliomas of histologic grade 2 and 3 follow heterogenous clinical outcomes, which necessitates risk stratification. This study aimed to evaluate whether diffusion-weighted and perfusion-weighted MRI radiomics allow overall survival (OS) prediction in patients with lower-grade gliomas and investigate its prognostic value.

Methods

In this retrospective study, radiomic features were extracted from apparent diffusion coefficient, relative cerebral blood volume map, and Ktrans map in patients with pathologically confirmed lower-grade gliomas (January 2012 – February 2019). The radiomics risk score (RRS) calculated from selected features constituted a radiomics model. Multivariable Cox regression analysis, including clinical features and RRS, were performed. The models' integrated area under the receiver operating characteristic curves (iAUC) were compared. The radiomics model combined with clinical features was presented as a nomogram.

Results

The study included 129 patients (median age, 44 years; interquartile range, 37–57 years; 66 women): 90 patients for training, and 39 patients for test set. The RRS was an independent risk factor for OS with a hazard ratio of 6.01. The combined clinical and radiomics model achieved superior performance for OS prediction compared to the clinical model in both training (iAUC, 0.82 vs. 0.72, *P* = .002) and test sets (0.88 vs. 0.76, *P* = .04). The radiomics nomogram combined with clinical features exhibited good agreement between the actual and predicted OS with C-index of 0.83 and 0.87 in the training and test set, respectively.

Conclusion

Adding diffusion- and perfusion-weighted MRI radiomics to clinical features improved survival prediction in lower-grade glioma.

Introduction

Lower-grade gliomas of World Health Organization (WHO) CNS grade 2 and 3 are infiltrative neoplasms with variable clinical outcomes, with widely ranging survival, from 1 to 15 years[1]. Isocitrate dehydrogenase (IDH) is one of the key genetic events leading to glioma stratification with significantly

different survival rates in adult-type diffuse gliomas[2,3]. However, heterogenous clinical outcomes have been reported in lower-grade gliomas with or without IDH mutation, according to the variable combination of genetic profiles[4,5]. Therefore, it would be beneficial if MRI could stratify lower-grade glioma patients according to their risk and identify patients with worse prognosis, better addressing specific treatment needs.

Physiological biomarkers from diffusion-weighted imaging (DWI) and perfusion-weighted imaging (PWI) have been largely investigated in patients with gliomas. The DWI-derived apparent diffusion coefficient (ADC) reflects cellularity within the tumor. Dynamic susceptibility contrast (DSC) imaging allows for the measurement of cerebral blood volume (CBV), a surrogate marker for vascular proliferation and tumor angiogenesis, whereas dynamic contrast-enhanced (DCE) imaging allows the evaluation of the blood-brain barrier integrity by measuring quantitative permeability parameters[6]. Advanced MRI protocols involving DWI, DSC, or DCE can potentially discriminate grades or predict specific genetic mutations or prognosis in patients with gliomas[7–9].

Radiomics exploits MRI data extracting high-dimensional quantitative imaging features such as intensity distributions, spatial relationships, textural heterogeneity, and shape descriptors[10]. Since radiomics models use high-throughput imaging features, hidden information, which may be visually imperceptible, can be revealed[11]. Conventional MRI-derived radiomics has been adopted in patients with lower-grade gliomas to detect molecular subtypes including IDH mutation status, predict survival, or responses from chemotherapeutic agents[12–15]. Previous studies using DWI or PWI radiomics showed that these advanced MRI radiomics had good performance in determining the tumor grade or predicting specific genetic mutations in lower-grade gliomas[16,17]. However, to the best of our knowledge, the prognostic significance of DWI or PWI radiomics to predict survival in patients with lower-grade gliomas has not been well investigated.

We hypothesized that MRI radiomics derived from ADC and perfusion maps could improve the survival prediction of clinical profiles in patients with lower-grade gliomas. Therefore, this study aimed to evaluate whether radiomics allow risk stratification in preoperative settings in patients with lower-grade gliomas and to investigate the added prognostic value of DWI or PWI radiomics over clinical features alone.

Materials And Methods

This retrospective study was approved by the Ethics Committee of Severance hospital (4-2021-1665). Given the retrospective nature of this study and the fact that no samples were obtained from human bodies, the requirement for informed consent was waived by the Ethics Committee of Severance hospital. In addition, all experiments were performed in accordance with relevant institutional and national guidelines and regulations.

Patients

From January 2012 to February 2019, 283 patients with pathologically confirmed lower-grade gliomas were identified. Patients with lower-grade gliomas who underwent preoperative MRI were included. Patients were excluded if they presented any of the following: 1) previous history of brain surgery or treatment (i.e. radiation therapy or chemotherapy, n = 21); 2) age < 18-years-old (n = 16); 3) no preoperative MRI (n = 12); 4) no DWI in the preoperative MRI (n = 4); 5) either DSC or DCE not available in the preoperative MRI (n = 99); 6) Error in preprocessing (n = 2). Thus, 129 patients with lower-grade gliomas and preoperative MRI including DWI, DSC, and DCE were enrolled in this study (Supplementary Fig. 1). Among them, 54 (41.9%) had WHO grade II gliomas and 75 (58.1%) had grade III gliomas.

Patients who had a pathologic diagnosis between 2015–2019 and 2012–2014 were allocated to the training and test sets, respectively.

The extent of tumor resection was determined by visually comparing the preoperative and postoperative lesion volume on both fluid-attenuated inversion recovery (FLAIR) and contrast-enhanced T1-weighted imaging (T1C), in conjunction with the surgeons' intraoperative impressions, classified into one of three categories: gross total, subtotal (< 100% and ≥ 75% of gross tumor removal)/partial (< 75% of gross tumor removal) resection, or biopsy only. The Karnofsky performance status (KPS) was determined preoperatively and retrieved from the electronic medical records.

Overall survival (OS) was used as a clinical outcome, and defined as the number of days from the initial surgery, i.e., tumor resection or biopsy, to either patient death or the date of the last follow-up.

Pathologic evaluation and molecular subtyping

All surgical specimens were histopathologically diagnosed according to the 2016 WHO classification. Both peptide nucleic acid-mediated clamping polymerase chain reaction and immunohistochemical analyses were performed to detect the presence of a IDH1-R132H mutation[2]. Monoclonal antibody H09 was used for immunohistochemical analysis. The degree of IDH1-R132H staining was determined positive if there were any stained cells. Cases without IDH1-R132H staining were determined to be negative[18,19]. In IDH1-negative cases, IDH1/2 status was confirmed by a peptide nucleic acid-mediated clamping polymerase chain reaction.

MR image acquisition and perfusion MRI preprocessing

The detailed MR image acquisition parameters and the preprocessing steps of DCE and DSC MRI are presented in the Supplementary Material S1. Ktrans map from DCE MRI and relative CBV (rCBV) map from DSC MRI were used for further analysis.

Image pre-processing and radiomic feature extraction

FLAIR and ADC preprocessing was performed to standardize data analysis among patients. A 1-mm isovoxel resampling of the images was performed with bias field correction via the N4 bias field correction algorithm. Signal intensity normalization was performed by applying the z-score. Preprocessing of the rCBV map and Ktrans map only included 1-mm isovoxel resampling. Tumor

segmentation was performed by a neuroradiologist with 7 years of experience, and confirmed by another senior neuroradiologist with 14 years of experience, both blinded to the clinical information. Semiautomatic segmentation was performed using the 3D slicer software (version 4.11.0). ADC images were co-registered to FLAIR images.

Radiomic features extracted from each mask were calculated automatically with an open-source python-based module (PyRadiomics, version 2.0)[20], adherent to the Image Biomarker Standardization Initiative[21]. The features included: (1) 14 shape features; (2) 18 first-order features; and (3) 75 second-order features, including gray level co-occurrence matrix (GLCM), gray level run-length matrix (GLRLM), gray level size zone matrix (GLSZM), gray level dependence matrix (GLDM), and neighboring gray tone difference matrix (NGTDM). Overall, 107 radiomic features were extracted from each sequence. Among them, 14 shape features were identical along different sequences. Therefore, 293 features were extracted from ADC, and the rCBV and Ktrans maps. The pipelines for radiomics feature extraction are presented in Supplementary Fig. 2.

Construction of the radiomics risk score

Because of the relatively large number of imaging variables compared with the number of events, the least absolute shrinkage and selection operator was used to select important features to minimize the potential risk for overfitting by shrinking the regression coefficients of irrelevant variables toward zero[22]. The performance of these methods was tested by 10-fold cross-validation with 100 replications to enhance the generalizability of the results. A radiomics risk score (RRS) was calculated for each patient using a linear combination of frequently selected features, weighted according to their regression coefficients. The RRSs calculated from selected features from the ADC and from both CBV and Ktrans maps constituted a DWI radiomics and PWI radiomics model, respectively.

Model development based on multivariable Cox regression analysis

Univariable analysis of RRS and clinicopathologic features—age, sex, KPS, postoperative treatment (i.e. chemotherapy or radiation therapy), extent of resection, IDH mutation status, and WHO grade —for OS prediction was performed. All the features except postoperative treatment were significantly associated with OS, and subsequently included for multivariable Cox regression analyses to create prognostic models: 1) clinical model – age, sex, and KPS, 2) clinicopathologic model – age, sex, KPS, extent of resection, IDH mutation status, and WHO grade, 3) combined clinical and radiomics model. To assess and compare model performance, the integrated area under the curve (iAUC) from a time-dependent receiver operating characteristic (ROC) curve[23] and the C-index of each model were calculated. Differences in those metrics between models were tested based on a 95% confidence interval (CI) from a bootstrap with 1,000 resampling. The difference was considered statistically significant if the 95% CI of the difference did not contain a zero value.

Construction of the radiomics nomogram

Based on the multivariable Cox regression, a radiomics nomogram integrating the RRS and clinical features was constructed to predict OS[24]. The discriminative ability of the nomogram was quantitatively measured using the C-index. The calibration curves were plotted using the observed probabilities and the nomogram-estimated probabilities in both training and test sets[25].

Statistical analysis

Statistical analysis was performed in R software (version 3.5.1; R Foundation for Statistical Computing, Vienna, Austria). For comparisons between the training and test set, student's t test, and either chi-square test or Fisher's exact test were performed for continuous and categorical variables, respectively. The LASSO analysis was based on the glmnet package. The optimal cut-off values of the RRSs were defined by the log-rank test, using the Contal and O'Quigley's method, performed using the "cutp" function of "survMisc" in R[26]. Patients in the training and test set were then classified into low-risk and high-risk groups according to a fixed cut-off value derived from the training set, and the Kaplan-Meier curves from both groups in the training and test sets were compared. The nomogram and calibration curves were established using the rms package. A P value < 0.05 was considered statistically significant.

Results

The characteristics of the 129 enrolled patients are summarized in Table 1. In the training and test set, the median OS was 961 days (interquartile range, 737–1543 days) and 2251 days (interquartile range, 1593–2482 days), respectively. There were no significant differences in clinicopathologic characteristics between the training and test sets.

Table 1
Patient characteristics in both training and test sets

Clinical Characteristics	Training set (n = 90)	Test set (n = 39)	P value
Age (years)	46.3 (13.6)	45.8 (12.0)	0.845
Sex (male:female)	46:44	20:19	> 0.999
Karnofsky Performance Status	90.0 (11.2)	90.0 (13.9)	0.374
Extent of resection			0.056
Total	32 (35.6%)	22 (56.4%)	
Subtotal or partial	43 (47.8%)	16 (41.0%)	
Biopsy	15 (16.7%)	1 (2.6%)	
WHO grade			
Grade 2	33 (26.7%)	21 (53.8%)	.11
Grade 3	57 (63.3%)	18 (46.2%)	
IDH mutation status			.19
IDH-mutant	68 (73.9%)	19 (51.4%)	
IDH-wild type	24 (26.1%)	18 (48.6%)	
Overall survival (Median, interquartile range)	961 (737–1543)	2251 (1593–2482)	.20
No. of deaths observed	26 (28.9%)	13 (33.3%)	.77

Numbers in parenthesis are standard deviation, otherwise specified. WHO = World Health Organization, IDH = Isocitrate dehydrogenase

Radiomics risk score construction

In the training set, the C-indices of three different radiomics models—1) single DWI radiomics, 2) single PWI radiomics, and 3) combined DWI and PWI radiomics—for OS prediction were 0.75 (95% confidence interval [CI] 0.64–0.86), 0.753 (95% CI, 0.65–0.85), and 0.81 (95% CI, 0.71–0.89), respectively. Since the combined DWI and PWI radiomics performed better than other single layer radiomics, this was used for further analysis. An RRS derived from 14 selected radiomic features (4 from ADC, 5 from DSC, and 5 from DCE) constituted a combined DWI and PWI radiomics. Detailed descriptions of selected features are presented in Supplementary Material S2.

The optimal RRS cut-off value, 1.68, was derived from the training set. This cut-off stratified both the training and test set into low-risk and high-risk group with statistically different OS (P < .001, both;

Supplementary Fig. 3).

Model development and performance evaluation

Multivariate Cox regression analysis created three models (clinical model, clinicopathologic model, and a combined clinical and radiomics model); the hazard ratio (HR) of each variable in the training set is presented in Table 2. Older age and lower KPS were significantly associated with worse prognosis, as observed in all three models. In the clinicopathologic model, IDH mutation status was the most powerful prognostic factor with an HR of 0.14. In the combined clinical and radiomics model, RRS was significantly associated with OS with an HR of 6.01.

Table 2
Three models created from multivariate Cox regression analysis in the training set

	Clinical model		**Clinicopathologic model**		**Clinical + DWI and PWI radiomics**	
Variables	HR (95% CI)	P-value	HR (95% CI)	P-value	HR (95% CI)	P-value
Age	1.04 (1.01–1.07)	.004	1.03 (1.00–1.06)	.04	1.04 (1.00–1.07)	.03
Gender	1.27 (0.58–2.77)	.55	1.06 (0.47–2.39)	.90	1.11 (0.450–2.45)	.78
KPS	0.94 (0.91–0.98)	.001	0.95 (0.91–0.98)	.005	0.96 (0.93–0.99)	.048
Extent of resection			2.29 (0.63–8.29)	.21	2.39 (0.69–8.27)	.17
WHO grade			1.94 (0.66–5.70)	.23		
IDH mutation status			0.14 (0.05–0.39)	< .001		
RRS					6.01 (2.60–13.86)	< .001
C-index	0.73 (0.65–0.85)		0.86 (0.80–0.94)		0.83 (0.75–0.92)	

DWI = Diffusion-weighted image, PWI = Perfusion-weighted image, HR = Hazard ratio, CI = Confidence interval, KPS = Karnofsky Performance Status, RRS = Radiomics risk score

The C-indices of those three different models are presented in Table 3. In the training set, adding DWI and PWI to the clinical model significantly increased the performance from 0.73 (95% CI, 0.65–0.85) to 0.83 (95% CI, 0.75–0.92). In the test set, adding DWI and PWI to a clinical model also significantly increased the performance from 0.75 (0.64–0.91) to 0.87 (0.80–0.98). In addition, the comparison between the C-index of the combined clinical and radiomics and the clinicopathologic model, which included well-known

powerful prognostic factors, i.e., WHO grade and IDH mutation status, showed no significant differences either in the training or test set.

Table 3
The C-indices of the various models for overall survival prediction in training and test sets

	Training set		Test set	
	C-index	Difference	C-index	Difference
Clinical + DWI and PWI radiomics	0.83 (0.75–0.92)	Reference	0.87 (0.80–0.98)	Reference
Clinical model	0.73 (0.65–0.85)	0.10 (0.02–0.20)	0.75 (0.64–0.91)	0.12 (0.01–0.25)
Clinicopathologic model	0.86 (0.80–0.94)	-0.03 (-0.08–0.05)	0.86 (0.87–0.99)	0.01 (-0.06–0.12)
DWI = Diffusion weighted image, PWI = Perfusion weighted image				

Time-dependent ROC curves from the clinical and the combined clinical and radiomics model are shown in Fig. 1. In the training set, the iAUC was significantly higher in the combined model than in the clinical model (0.82 [95% CI, 0.78–0.82] vs. 0.72 [95% CI, 0.68–0.72]). On bootstrap testing, the increase in iAUC (0.10 [95% CI, 0.07–0.12]) was statistically significant. Similarly, in the test set, when radiomics was added to the clinical model, the iAUC significantly increased from 0.76 (95% CI, 0.64–0.87) to 0.88 (95% CI, 0.80–0.96), with the increase in iAUC (0.12 [95% CI, 0.03–0.24]) being statistically significant.

Radiomics nomogram construction and validation

A radiomics nomogram incorporating the RRS and clinical features was constructed based on multivariate logistic regression (Fig. 2). The corresponding calibration curves demonstrated satisfactory consistency between the nomogram-predicted survival and the actual observed survival in both the training (C-index, 0.83 [95% CI, 0.75–0.92]) and test set (C-index, 0.87 [95% CI, 0.80–0.98]).

Discussion

In this study, radiomics derived from advanced MRI such as DWI and PWI was used to predict survival in patients with lower-grade gliomas. We observed that radiomics derived from both DWI and PWI, rather than single layer radiomics, performed better for OS prediction. The optimal RRS cut-off derived from the training set divided the test set into two groups with significantly different survival outcomes, demonstrating the RRS' prognostic value. Further, adding DWI and PWI radiomics to clinical features significantly increased model performance for OS prediction, as validated in the test set. Calibration curves proved the prognostic accuracy of a nomogram constructed from clinical features and radiomics. Our study, therefore, suggests that DWI and PWI radiomics may allow non-invasive risk stratification of patients with lower-grade gliomas and can be used as a potential imaging biomarker.

Little has been studied regarding the prognostic value of advanced MRI radiomics, from either DWI or PWI. Previous studies used advanced MRI radiomics to predict tumor grade and specific genetic mutation status in lower-grade gliomas. The radiomics derived from an ADC map, not FLAIR, provided the highest prediction accuracy for determining the IDH mutation status[17]. Furthermore, most of the top contributing features for the prediction of tumor grades were derived from the ADC map[16]. Multiparametric MRI radiomics including conventional MRI, ADC, and CBV also outperformed conventional MRI radiomics in tumor grading[16]. Hence, we focused on the added prognostic role of advanced MRI radiomics, rather than conventional MRI radiomics, over clinical features in patients with lower-grade gliomas. We observed that the RRS from advanced MRI radiomics was one of the independent risk factors for survival prediction. The combined clinical and radiomics model achieved superior performance for OS prediction compared to the clinical model, with iAUC being 0.883 in the test set. Further, the performance of the combined model was comparable to that of the clinicopathologic model including the IDH mutation status, one of the most powerful prognostic factors that can be obtained after invasive surgery.

Numerous studies investigated the prognostic role of perfusion MRI in patients with gliomas, mostly focusing on patients with glioblastomas. The rCBV and Ktrans, obtained from DSC and DCE MRI respectively, were frequently reported to significantly negatively correlate with survival, thereby having potential as imaging biomarkers for risk stratification[27–29]. Recently, radiomics has been applied to the rCBV or Ktrans map, showing that perfusion MRI radiomics provided useful information for predicting survival[30], improved prognostication over clinical features[31], had significant association with recurrence or progression, and enabled prediction of recurrence pattern[32] in patients with glioblastomas. Even perfusion MRI radiomics derived from nonenhancing, T2 hyperintense lesions of glioblastomas can also predict prognosis and had a significant association with progression-free survival or OS[33]. However, little is known about the prognostic role of perfusion MRI radiomics in lower-grade gliomas. In our study, a single layer perfusion MRI radiomics alone, derived from both rCBV and Ktrans map, could accurately predict OS with C-index of 0.753 in the training set. Furthermore, among 14 selected features which constituted a combined DWI and PWI radiomics, 10 were from either rCBV or Ktrans map. Therefore, we believe that PWI radiomics play a significant role in OS prediction not only in glioblastomas but also in patients with lower-grade gliomas. Finally, a combined DWI and PWI radiomics model achieved high accuracy for OS prediction when added to clinical features, which proved the added prognostic value of PWI radiomics in patients with lower-grade gliomas.

We then constructed a nomogram from the combined clinical and radiomics model for OS prediction, including age, gender, KPS, and radiomics derived from both DWI and PWI. A previous study using an independently validated nomogram in lower-grade gliomas concluded that grade 2 tumor, younger age at diagnosis, having a high KPS, and the IDH mutant, 1p19q-codeleted molecular subtype increased the probability of survival[34]. This nomogram included clinically relevant pathologic features such as WHO grade and molecular subtype. In our study, we only included features available in the preoperative setting, so that the nomogram can calculate individualized survival probabilities before surgery. In addition, DWI

and PWI radiomics from preoperative MRI were added. It was proven to have an effective tool for providing individualized survival probabilities with a C-index of 0.833 in the test set and good calibration.

The top contributing feature for the OS prediction was the skewness from ADC, a first order feature. Skewness, a histogram parameter, denotes an asymmetric distribution. As lower ADC values and their heterogeneity reflect increased tumor cellularity and heterogeneity[35], ADC skewness may have a significant association with survival. Among 14 selected features, half were texture features, which quantify the image pattern on the basis of the spatial relationship or co-occurrence of pixel values[36] and provide information on intratumoral heterogeneity[10]. As in gliomas intratumoral heterogeneity has been reportedly associated with aggressive tumor behaviour and drug resistance[37], texture features may play a key role in predicting prognosis.

There are several limitations in this study. First, it is a retrospective study with a relatively small sample size, because only patients with lower-grade glioma with both preoperative DSC and DCE MRI were included. Identification of an external validation set with patients with those same characteristics was not feasible; therefore, we performed temporal validation. Further studies using a larger cohort are required to validate our results. Second, important prognostic molecular markers such as epidermal growth factor receptor amplification or telomerase reverse transcriptase gene promoter mutation were not included in the analysis due to lack of information in a considerable number of patients. Future studies may validate the prognostic role of advanced MRI radiomics in consideration of those important molecular markers.

In conclusion, diffusion- and perfusion-weighted MRI radiomics enables non-invasive risk stratification and can improve survival prediction when added to the clinical features in patients with lower-grade gliomas.

Abbreviations

ADC Apparent diffusion coefficient

DCE Dynamic contrast-enhanced

DSC Dynamic susceptibility contrast

DWI Diffusion-weighted imaging

iAUC Integrated area under the receiver operating characteristic curve

IDH Isocitrate dehydrogenase

KPS Karnofsky Performance Status

OS Overall survival

ROC Receiver operating characteristics

RRS Radiomics risk score

Declarations

Acknowledgements

Funding information: This research received funding from the Basic Science Research Program through the National Research Foundation of Korea (NRF) funded by the Ministry of Science, Information and Communication Technologies & Future Planning (2020R1A2C1003886) and a grant from the Korea Health Technology R&D Project through the Korea Health Industry Development Institute, funded by the Ministry of Health & Welfare, Republic of Korea (HI21C1161).

Author Contributions

All authors contributed to the study conception and design. Material preparation and data collection were performed by Chae Jung Park, Sung Soo Ahn, Yae Won Park, and Jong Hee Chang. The analysis was performed by Sooyon Kim and Kyunghwa Han. The first draft of the manuscript was written by Chae Jung Park, Se Hoon Kim, and Seung-Koo Lee. The manuscript revision was made by Sung Soo Ahn, Jong Hee Chang, Se Hoon Kim, and Seung-Koo Lee. All authors commented on previous versions of the manuscript. All authors read and approved the final manuscript.

Competing interests

The author(s) declare no competing interests.

Data Availability

The datasets generated during and/or analysed during the current study are available from the corresponding author on reasonable request.

References

1. Brat, D. J. *et al.* Comprehensive, Integrative Genomic Analysis of Diffuse Lower-Grade Gliomas. N Engl J Med **372**, 2481–2498. https://doi.org/10.1056/NEJMoa1402121 (2015).
2. Yan, H. *et al.* IDH1 and IDH2 mutations in gliomas. N Engl J Med **360**, 765–773. https://doi.org/10.1056/NEJMoa0808710 (2009).
3. Louis, D. N. *et al.* The 2021 WHO Classification of Tumors of the Central Nervous System: a summary. Neuro-Oncology **23**, 1231–1251. https://doi.org/10.1093/neuonc/noab106 (2021).
4. Aibaidula, A. *et al.* Adult IDH wild-type lower-grade gliomas should be further stratified. Neuro Oncol **19**, 1327–1337. https://doi.org/10.1093/neuonc/nox078 (2017).
5. Brat, D. J. *et al.* cIMPACT-NOW update 3: recommended diagnostic criteria for "Diffuse astrocytic glioma, IDH-wildtype, with molecular features of glioblastoma, WHO grade IV". Acta

neuropathologica **136**, 805–810. https://doi.org/10.1007/s00401-018-1913-0 (2018).

6. van Dijken, B. R. J. *et al.* Perfusion MRI in treatment evaluation of glioblastomas: Clinical relevance of current and future techniques. J Magn Reson Imaging **49**, 11–22. https://doi.org/10.1002/jmri.26306 (2019).
7. Choi, Y. S. *et al.* The Initial Area Under the Curve Derived from Dynamic Contrast-Enhanced MRI Improves Prognosis Prediction in Glioblastoma with Unmethylated MGMT Promoter. AJNR Am J Neuroradiol **38**, 1528–1535. https://doi.org/10.3174/ajnr.A5265 (2017).
8. Villanueva-Meyer, J. E. *et al.* MRI Features and IDH Mutational Status of Grade II Diffuse Gliomas: Impact on Diagnosis and Prognosis. AJR Am J Roentgenol **210**, 621–628. https://doi.org/10.2214/ajr.17.18457 (2018).
9. Leu, K. *et al.* Perfusion and diffusion MRI signatures in histologic and genetic subtypes of WHO grade II-III diffuse gliomas. J Neurooncol **134**, 177–188. https://doi.org/10.1007/s11060-017-2506-9 (2017).
10. Gillies, R. J., Kinahan, P. E. & Hricak, H. Radiomics: Images Are More than Pictures, They Are Data. Radiology **278**, 563–577. https://doi.org/10.1148/radiol.2015151169 (2016).
11. Aerts, H. J. *et al.* Decoding tumour phenotype by noninvasive imaging using a quantitative radiomics approach. Nat Commun **5**, 4006. https://doi.org/10.1038/ncomms5006 (2014).
12. Park, C. J. *et al.* MRI Features May Predict Molecular Features of Glioblastoma in Isocitrate Dehydrogenase Wild-Type Lower-Grade Gliomas. AJNR Am J Neuroradiol **42**, 448–456. https://doi.org/10.3174/ajnr.A6983 (2021).
13. Park, C. J. *et al.* Radiomics risk score may be a potential imaging biomarker for predicting survival in isocitrate dehydrogenase wild-type lower-grade gliomas. Eur Radiol **30**, 6464–6474. https://doi.org/10.1007/s00330-020-07089-w (2020).
14. Choi, Y. S. *et al.* Machine learning and radiomic phenotyping of lower grade gliomas: improving survival prediction. Eur Radiol **30**, 3834–3842. https://doi.org/10.1007/s00330-020-06737-5 (2020).
15. Wang, J. *et al.* An MRI-based radiomics signature as a pretreatment noninvasive predictor of overall survival and chemotherapeutic benefits in lower-grade gliomas. Eur Radiol **31**, 1785–1794. https://doi.org/10.1007/s00330-020-07581-3 (2021).
16. Kim, M. *et al.* Diffusion- and perfusion-weighted MRI radiomics model may predict isocitrate dehydrogenase (IDH) mutation and tumor aggressiveness in diffuse lower grade glioma. Eur Radiol **30**, 2142–2151. https://doi.org/10.1007/s00330-019-06548-3 (2020).
17. Ren, Y. *et al.* Noninvasive Prediction of IDH1 Mutation and ATRX Expression Loss in Low-Grade Gliomas Using Multiparametric MR Radiomic Features. J Magn Reson Imaging **49**, 808–817. https://doi.org/10.1002/jmri.26240 (2019).
18. Takano, S. *et al.* Detection of IDH1 mutation in human gliomas: comparison of immunohistochemistry and sequencing. Brain Tumor Pathol **28**, 115–123. https://doi.org/10.1007/s10014-011-0023-7 (2011).

19. Choi, J. *et al.* IDH1 mutation analysis in low cellularity specimen: a limitation of diagnostic accuracy and a proposal for the diagnostic procedure. Pathol Res Pract **209**, 284–290. https://doi.org/10.1016/j.prp.2013.02.010 (2013).
20. van Griethuysen, J. J. M. *et al.* Computational Radiomics System to Decode the Radiographic Phenotype. Cancer Res **77**, e104-e107. https://doi.org/10.1158/0008-5472.Can-17-0339 (2017).
21. Zwanenburg, A. *et al.* The Image Biomarker Standardization Initiative: Standardized Quantitative Radiomics for High-Throughput Image-based Phenotyping. Radiology **295**, 328–338. https://doi.org/10.1148/radiol.2020191145 (2020).
22. Friedman, J., Hastie, T. & Tibshirani, R. Regularization Paths for Generalized Linear Models via Coordinate Descent. J Stat Softw **33**, 1–22 (2010).
23. Heagerty, P. J. & Zheng, Y. Survival model predictive accuracy and ROC curves. Biometrics **61**, 92–105. https://doi.org/10.1111/j.0006-341X.2005.030814.x (2005).
24. Iasonos, A., Schrag, D., Raj, G. V. & Panageas, K. S. How to build and interpret a nomogram for cancer prognosis. J Clin Oncol **26**, 1364–1370. https://doi.org/10.1200/jco.2007.12.9791 (2008).
25. Balachandran, V. P., Gonen, M., Smith, J. J. & DeMatteo, R. P. Nomograms in oncology: more than meets the eye. Lancet Oncol **16**, e173-180. https://doi.org/10.1016/s1470-2045(14)71116-7 (2015).
26. *Computational Statistics & Data Analysis* **30**, 253–270 (1999).
27. Schmainda, K. M. *et al.* Dynamic susceptibility contrast MRI measures of relative cerebral blood volume as a prognostic marker for overall survival in recurrent glioblastoma: results from the ACRIN 6677/RTOG 0625 multicenter trial. Neuro Oncol **17**, 1148–1156. https://doi.org/10.1093/neuonc/nou364 (2015).
28. Larsson, C. *et al.* Prediction of survival and progression in glioblastoma patients using temporal perfusion changes during radiochemotherapy. Magnetic Resonance Imaging **68**, 106–112. https://doi.org/https://doi.org/10.1016/j.mri.2020.01.012 (2020).
29. Bonekamp, D. *et al.* Association of overall survival in patients with newly diagnosed glioblastoma with contrast-enhanced perfusion MRI: Comparison of intraindividually matched T1- and T2*-based bolus techniques. Journal of Magnetic Resonance Imaging **42**, 87–96. https://doi.org/https://doi.org/10.1002/jmri.24756 (2015).
30. Lee, J. *et al.* Texture Feature Ratios from Relative CBV Maps of Perfusion MRI Are Associated with Patient Survival in Glioblastoma. American Journal of Neuroradiology **37**, 37–43. https://doi.org/10.3174/ajnr.A4534 (2016).
31. Park, J. E. *et al.* Radiomics prognostication model in glioblastoma using diffusion- and perfusion-weighted MRI. Sci Rep **10**, 4250. https://doi.org/10.1038/s41598-020-61178-w (2020).
32. Shim, K. Y. *et al.* Radiomics-based neural network predicts recurrence patterns in glioblastoma using dynamic susceptibility contrast-enhanced MRI. Sci Rep **11**, 9974. https://doi.org/10.1038/s41598-021-89218-z (2021).
33. Pak, E. *et al.* Prediction of Prognosis in Glioblastoma Using Radiomics Features of Dynamic Contrast-Enhanced MRI. Korean J Radiol **22**, 1514–1524. https://doi.org/10.3348/kjr.2020.1433

(2021).

34. Gittleman, H., Sloan, A. E. & Barnholtz-Sloan, J. S. An independently validated survival nomogram for lower-grade glioma. Neuro-Oncology **22**, 665–674. https://doi.org/10.1093/neuonc/noz191 (2019).
35. Eidel, O. *et al.* Automatic Analysis of Cellularity in Glioblastoma and Correlation with ADC Using Trajectory Analysis and Automatic Nuclei Counting. PLoS One **11**, e0160250. https://doi.org/10.1371/journal.pone.0160250 (2016).
36. Soni, N., Priya, S. & Bathla, G. Texture Analysis in Cerebral Gliomas: A Review of the Literature. AJNR Am J Neuroradiol **40**, 928–934. https://doi.org/10.3174/ajnr.A6075 (2019).
37. Meyer, M. *et al.* Single cell-derived clonal analysis of human glioblastoma links functional and genomic heterogeneity. Proc Natl Acad Sci U S A **112**, 851–856. https://doi.org/10.1073/pnas.1320611111 (2015).

Figures

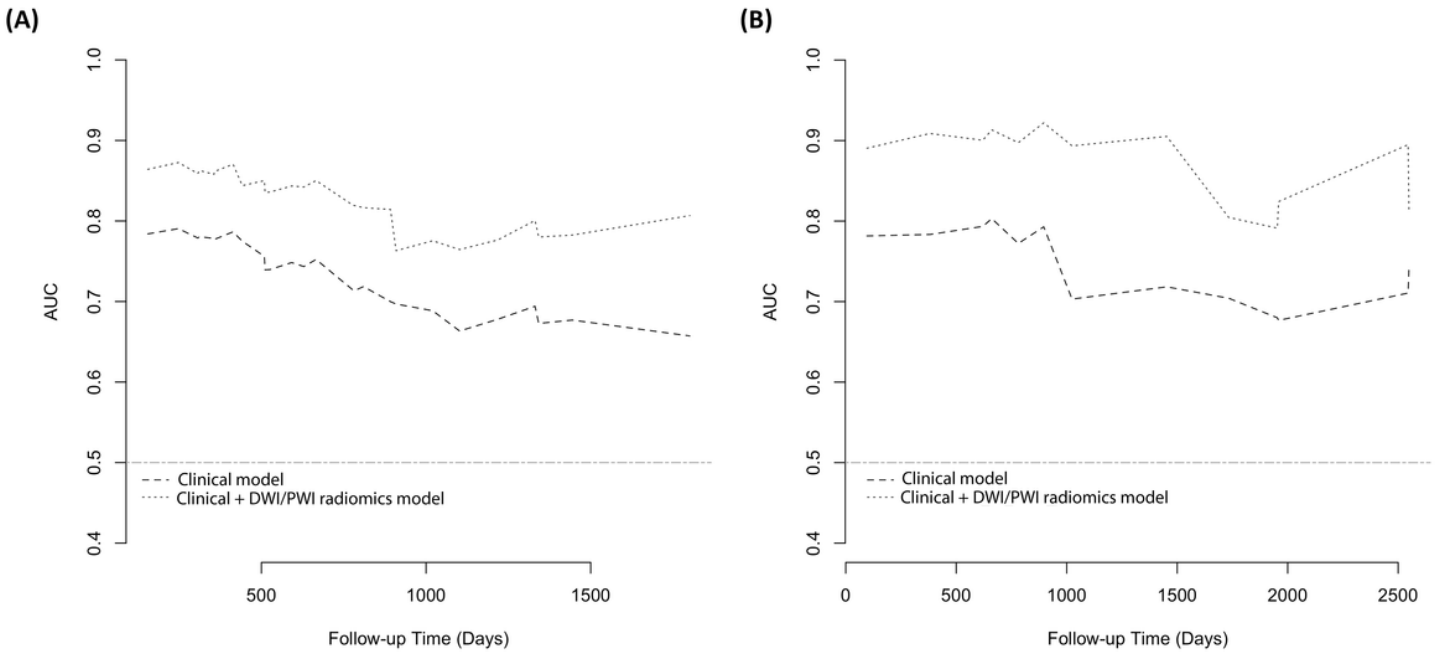

Figure 1

Time-dependent receiver operating characteristic curves from a clinical model and a combined clinical and radiomics model in (**a**) training and (**b**) test set

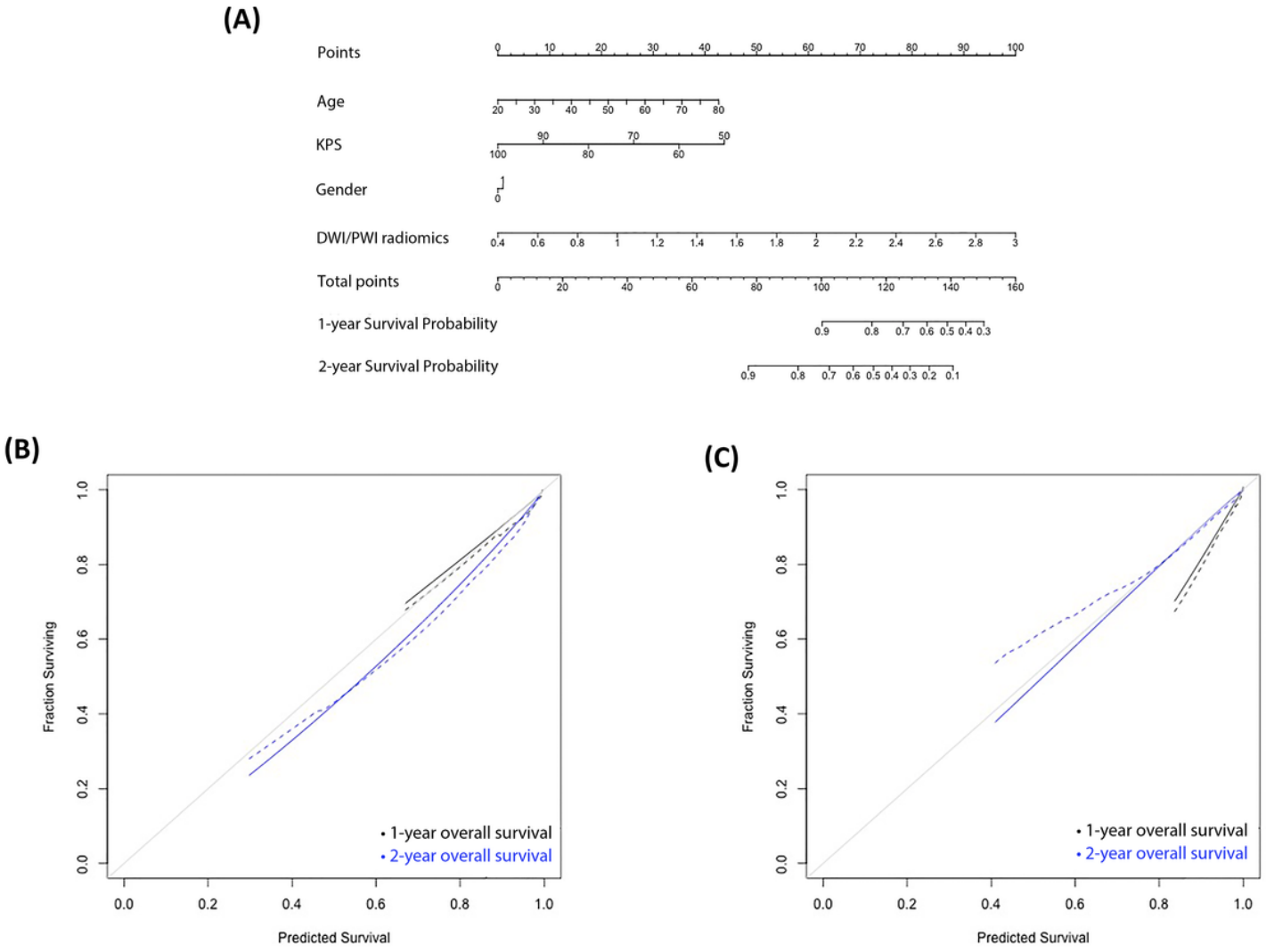

Figure 2

Nomogram derived from a combined clinical and radiomics model for the prediction of overall survival (**a**). Calibration curves of the nomogram in the training (**b**) and test cohort (**c**) demonstrated good consistency between the nomogram-estimated and actual overall survival

Supplementary Files

This is a list of supplementary files associated with this preprint. Click to download.

- SupplementaryInformationFinal.docx